PALLADIUM AND PLATINUM ISOTOPIC COMPOSITION OF CHONDRITES AND IRON METEORITES. S. Sharma[1], M. Humayun[1] and I. Leya[2]. [1]Dept. Earth, Ocean & Atmospheric Science, and National High Magnetic Field Laboratory, Florida State University, Tallahassee, FL 32310, USA (ss18x@my.fsu.edu). [2]Space Research and Planetology, University of Bern, 3012 Bern, Switzerland.

Introduction: Nucleosynthetic anomalies in bulk meteorites have been identified in a number of refractory or moderately refractory elements (Ti, Cr, Ni, Zr, Mo, Ru, Pd, Ba, Nd, and Sm) but not in heavier elements such as Hf, Os, Pt or volatile elements such as Cd and Te [1-6]. Such anomalies reflect primordial heterogeneities that survived mixing in the proto-solar nebula either due to poor mixing of the carrier phases into the protoplanetary disk and/or their selective destruction via thermal processing in the disk [7].

Palladium, an element similar in volatility to Fe and Ni, has six naturally occurring stable isotopes—^{102}Pd, ^{104}Pd, ^{105}Pd, ^{106}Pd, ^{108}Pd, ^{110}Pd. ^{102}Pd is a p-process isotope, ^{104}Pd is a s-only isotope, ^{105}Pd, ^{106}Pd, ^{108}Pd are produced by both s- and r-processes, and ^{110}Pd is a r-process only isotope. Correlated ε^{104}Pd deficits and ε^{110}Pd excesses from IVB irons [2] and other iron groups have been reported [8,9].

Platinum has one s-process isotope (^{192}Pt) and five r-process isotopes (^{194}Pt, ^{195}Pt, ^{196}Pt, and ^{198}Pt). Prior studies have found no evidence of nucleosynthetic anomalies in Pt isotopes [10,11] but recently small isotopic anomalies were reported in some ungrouped iron meteorites [12]. Platinum isotopes have been used to correct for the effects of galactic cosmic ray (GCR) induced secondary neutron capture reactions on isotopic compositions of other elements, such as ^{103}Rh to yield ^{104}Pd, which must be corrected to obtain Pd nucleosynthetic anomalies [2,10]. This is based on an assumption that there are no nucleosynthetic isotopic anomalies in Pt isotopes so any deviations reflect cosmic ray exposure (CRE) effects.

In this study, we report the Pd and Pt isotope compositions of six different groups of iron meteorites- IAB (n=1, Campo del Cielo), IIAB (n=8), IID (n=1, NEA 002), IIIE (n=1, Aletai), IVA (n=1, Muonionalusta), and IVB (n=5), two ungrouped iron meteorites- Chinga and Gebel Kamil, and four carbonaceous chondrites- NWA 801 (CR2), NWA 8038 (CO3.5), Jbilet Winselwan (CM), and Gujba (CBa). Platinum isotopic compositions of the same aliquots were used to serve as an in-situ neutron dosimeter [10, 11, 13].

Analytical Methodology: Samples were analyzed for palladium and platinum isotopic composition using a Thermo Neptune™ MC-ICP-MS at the National High Magnetic Field Laboratory (NHMFL), Florida State University. All samples were dissolved using aqua regia in Savillex™ PFA beakers at 150°C. Two-stage chemical separation using a 15 mL cation exchange column, followed by a 2 mL anion exchange column was used to obtain pure Pd aliquots [2]. All Pd aliquots were analyzed with a Thermo Element 2™ ICP-MS to measure impurities (Zn, Zr, Ru, Cd etc.) prior to measurement on the MC-ICP-MS. The Pd cuts used for measurement had ^{101}Ru/^{105}Pd < 1x10^{-4}.

The isotopic acquisition was done in low resolution static mode collecting 5 blocks of 50 cycles each using about 100 ng/mL Pd aliquots in 2 % HCl introduced with a CETAC Aridus II desolvating nebulizer. The raw ratios were corrected for mass bias with the exponential law normalized to ^{108}Pd/^{105}Pd= 1.18899 [14]. Palladium isotopic composition is reported as ε^{i}Pd: $\varepsilon^{i}\text{Pd} = [(^{i}\text{Pd}/^{105}\text{Pd}_{sample})/(^{i}\text{Pd}/^{105}\text{Pd}_{ref})-1]\times10{,}000$, where i refers to 104, 106, and 110, relative to an Alfa Aesar® Specpure® Pd solution standard. Typical 2SE reproducibility for ε^{104}Pd, ε^{106}Pd, and ε^{110}Pd was ±0.05, ±0.02, and ±0.06 ε-units, respectively. While collecting Pd isotope compositions, isobaric interferences from Ru (^{101}Ru) and Cd (^{111}Cd) were simultaneously monitored on the MC-ICP-MS. Currently, measurement of ^{102}Pd is limited by the precision (2SE= ±0.80 ε).

The platinum isotopic composition is reported as ε^{i}Pt: $\varepsilon^{i}\text{Pt} = [(^{i}\text{Pt}/^{195}\text{Pt}_{sample})/(^{i}\text{Pt}/^{195}\text{Pt}_{ref})-1]\times10{,}000$, where i refers to 192, 194, and 196, relative to an Alfa Aesar® Specpure® Pt solution standard. The raw ratios were corrected for mass bias with the exponential law normalized to ^{198}Pt/^{195}Pt= 0.211740 [15]. Typical 2SE reproducibility for ε^{192}Pt, ε^{194}Pt, and ε^{196}Pt is ±0.50, ±0.05, and ±0.05 ε-units, respectively. For Pt aliquots, the measured ^{189}Os/^{195}Pt and ^{199}Hg/^{195}Pt ratios were lower than 8x10^{-5} and 1.1x10^{-4} respectively, which result in negligible corrections on ε^{192}Pt, ε^{194}Pt, and ε^{196}Pt.

Results: Fig. 1 shows the Pd isotope data reported in this study. Neutron capture corrections were made on ε^{104}Pd and ε^{110}Pd using ε^{196}Pt as an in-situ neutron dosimeter by combining respective Rh/Pd ratios with the model of [13]. The corrections for chondrites were negligible due to their low exposure ages. The choice of samples and the neutron dosimeter used to evaluate GCR corrections can alter the group average composition. The slope of ε^{104}Pd vs. ε^{110}Pd can vary depending on over- or under- correction of GCR effects [9]. Therefore, the IIAB and IVB group averages were calculated using the least irradiated samples (as evident from their Pt isotope compositions). The IIAB group average is based on the eight least irradiated samples: Ne-grillos, Coahuila, Gressk, Keen Mountain, North Chile, Park City, Uwet, and Braunau. The IVB group average was calculated using the five least irradiated samples:

Ternera, Warburton Range, Weaver Mountains, Tawal-lah Valley, and Skookum.

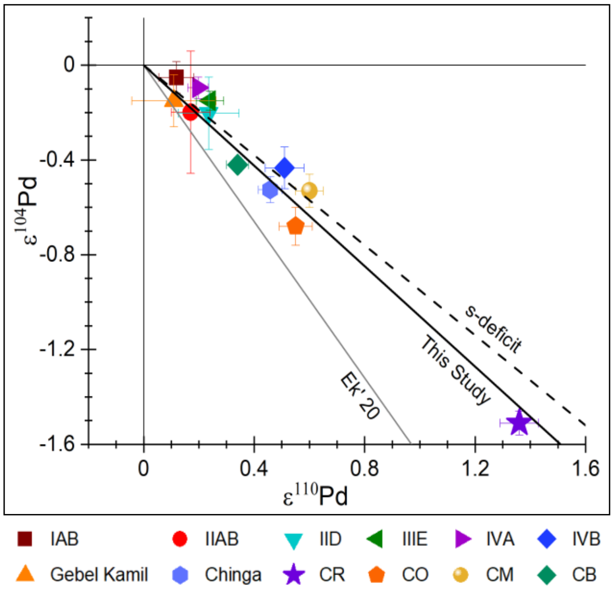

Fig. 1: A plot of ε^{104}Pd *vs* ε^{110}Pd for the samples reported in this study with the solid black regression line (m=-1.07, R^2=0.98). Dashed line shows the calculated s-deficit trend using the model of [16]. The solid gray trend line is the regression reported in previous study [8]. GCR corrections based on ε^{196}Pt (except Gebel Kamil and chondrite samples). Error bars are 2SE.

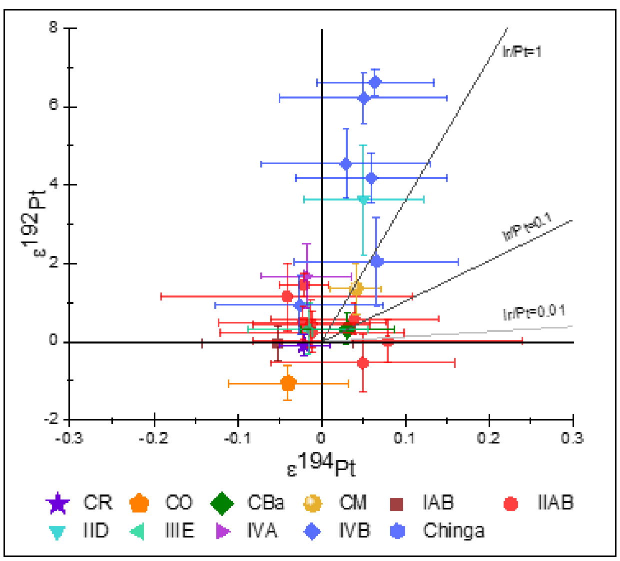

Fig. 2: A plot of ε^{192}Pt *vs* ε^{194}Pt. Solid gray lines represent modeled effects of GCR reactions for different Ir/Pt ratios. Error bars are 2SE.

The platinum isotopic composition of chondrites and iron meteorite groups are shown in Fig. 2.

Discussion: The isotopic composition of all meteorites analyzed show correlated anomalies in ε^{104}Pd and ε^{110}Pd attributed to variable s-process deficits between the different meteorite groups. The maximum s-deficit signature is exhibited by the CR carbonaceous chondrite, NWA 801, that is almost double that of any other meteorite yet observed. The maximum s-deficit signature amongst the iron meteorites is observed in IVB irons and Chinga, whereas the IAB group has a composition indistinguishable within error from the terrestrial value. The observed slope for the correlation between ε^{104}Pd and ε^{110}Pd (m=-1.07, R^2=0.98) lies between the s-deficit trend (m=-0.95) and the slope measured by [8] (m=-1.65).

CRE-induced isotope effects result in positive ε^{192}Pt, ε^{194}Pt, and ε^{196}Pt values due to neutron capture on ^{191}Ir, ^{193}Ir, and ^{195}Pt, respectively. We observe excesses in ε^{192}Pt and ε^{194}Pt consistent with the cosmogenic effects (Fig.2). Large isotopic shifts are observed in iron meteorites due to their long exposure ages and larger sizes. Chondrites do not have long exposure ages and are comparatively smaller in size, resulting in very small cosmogenic isotope anomalies. We do not observe nucleosynthetic platinum isotopic signature in chondrites or iron meteorites.

References: [1] Burkhardt C. et al. (2011) *EPSL*, *312*, 390-400. [2] Mayer B. et al. (2015) *ApJ*, 809, 180. [3] Akram et al. (2015) *GCA*, *165*, 484-500. [4] Fischer-Gödde M. et al. (2015) *GCA*, *168*, 151-171. [5] Bermingham K. et al. (2018) *EPSL*, 487, 221–229). [6] Nanne et al. (2019) *EPSL*, *511*, 44-54. [7] Bermingham et al. (2020) *Space Sci Rev*, 216:133. [8] Ek M. et al. (2020) *Nat Astron* 4, 273–281. [9] Sharma S. et al. (2021) *LPS LII*, Abstract #1655. [10] Wittig N. et al. (2013) *EPSL*, *361*, 152-161. [11] Kruijer T. et al. (2014) *Science*, *344*, 6188. [12] Spitzer F. et al. (2021) *EPSL*, 576, 117211. [13] Leya I. and Masarik J., 2013, *MAPS*, 48, 665-685. [14] Kelly W. R. and Wasserburg G. J., 1978, *GeoRL*, 5, 1079. [15] Rosman K.J.R. and Taylor P.D.P (1997) *SIAM*, pp1-22. [16] Arlandini et al. (1999) *ApJ*, *525*, 886-900.